

Supplementary Materials

for

Requirements for mammalian promoters to decode transcription factor dynamics

Enoch B. Antwi, Yassine Marrakchi, Özgün Çiçek, Thomas Brox, Barbara Di Ventura

Table of contents

Supplementary Text

Supplementary Tables S1-S7

Supplementary Figures S1-S10

Legend for Supplementary Video S1

Supplementary References

Supplementary Text

Mathematical model of gene expression in response to different synTF dynamics

We model the process of gene expression using a deterministic, two-compartment model, with eleven variables. The two compartments represent the cytosol and the nucleus, and the ten variables represent the following molecular species:

TF: cytosolic synTF

NTF: nuclear synTF

P_u: unbound promoter

P_a: active promoter

P_r: refractory promoter

PIC: pre-initiation complex

nRNA: nascent RNA

mRNA: mature mRNA

rbz: bound ribosome

iP: immature protein

mP: mature protein

We opted for a deterministic, instead of a stochastic model of gene expression, because our experimental setup is based on transient transfection of plasmid DNA, therefore, on average, there are more than two copies of the promoter of interest per cell; moreover, synTF is also expressed from the plasmid under the strong CMV promoter. We conclude that our species are present in medium copy and we can follow the average concentration of the species using ordinary differential equations (ODEs).

For each variable, we wrote an ODE that describes the change over time of its concentration.

The model consists of the following eleven ODEs describing cytosolic synTF [1], nuclear synTF [2], unbound promoter [3], active promoter [4], refractory promoter [5], PIC formation or stabilization [6], nascent RNA production [7], RNA maturation [8], bound ribosome [9], mRNA translation to immature protein [10], protein maturation [11], plus one equation that describes DNA looping efficiency [12].

The first two equations describe the change over time in the concentration of synTF in the cytoplasm and the nucleus:

$$\frac{dTF}{dt} = K_{TF} + darkrev(t) - lightAct(t) - d_{TF} * [TF] \quad [1]$$

$$\frac{dNTF}{dt} = lightAct(t) - darkrev(t) - d_{NTF} * [NTF] \quad [2]$$

K_{TF} , d_{TF} and d_{NTF} are constants that describe the *de novo* production rate and degradation rates of synTF in the cytosol and nucleus, respectively. Production occurs only in the cytoplasm, while degradation occurs in both compartments.

darkrev(t) and lightAct(t) are two functions that describe the export and import of synTF from/into the nucleus, respectively.

The lightAct(t) function is dependent on time (t), duration of activating blue light (tOn), duration of recovery phase in the dark (tOff), rates of synTF nuclear import during light activation (iOn) and dark recovery phase (iOff). We added this latter nuclear import in the dark to take into account the fact that the LOV domain is in equilibrium between its dark state, in which the C-terminal $J\alpha$ helix is folded and bound to the core domain, therefore shielding the NLS from the import machinery, and its lit state, characterized by an unfolded $J\alpha$ helix, which is further away from the core domain, letting the NLS be recognized (1). The duration of the light activation (lightdur) is defined in minutes. The function lightAct(t) is defined in python as shown below and returns synTF import rate (imp):

```
def lightAct(t, tOn, tOff, iOn, iOff):
    if (t <= lightdur):
        if (t%(tOn + tOff) < tOn):
            imp = iOn
        elif (t%(tOn + tOff) >= tOn):
            imp = iOff
        else:
            imp = iOff
    return(imp)
```

The darkrev(t) function is dependent on time (t), duration of activating blue light on (tOn), duration of recovery phase in the dark (tOff), rates of synTF export out of the nucleus during light activation (rOn) and dark phase (rOff). The function darkrev(t) is defined in python as shown below and returns synNTF export rate (exp):

```
def darkrev(t, tOn, tOff, rOn, rOff):
    if (t <= lightdur):
        if (t%(tOn + tOff) < tOn):
            exp = rOn
        elif (t%(tOn + tOff) >= tOn):
            exp = rOff
        else:
            exp = rOff
```

return(exp)

The next three equations describe the change over time in the promoter state. The promoter can assume three states: unbound (P_u), active (P_a) and refractory (P_r). It is only in the active state that the promoter is able to trigger transcription pre-initiation complex (PIC) assembly (described by equation 6). A three-state promoter model that includes a refractory state was necessary to account for the refractory behaviour seen in the nascent RNA data of some promoters. All promoter states are reversible.

Equation 3 describes the species P_u . P_u becomes P_a when bound by NTF. NTF binding to P_u is modelled as cooperative using a Hill function of NTF concentration multiplied by the constant K_{on} , where m is the Hill coefficient and kD_1 is the affinity of synTF for the RE. The change over time of P_u concentration also depends of the rate at which P_a and P_r revert back to the unbound state P_u (K_{off} and $d1_{rf}$, respectively):

$$\frac{dP_u}{dt} = K_{off} * P_a + d1_{rf} * P_r - K_{on} * \left(\frac{NTF^m}{kD_1^m + NTF^m} \right) * P_u \quad [3]$$

Equation 4 describes the species P_a . P_a is formed when P_u is bound by NTF. As mentioned above, NTF binding to P_u is modelled as cooperative using a Hill function of NTF concentration multiplied by the constant K_{on} , where m is the Hill coefficient and kD_1 is the affinity of synTF for the RE. P_a is additionally gained back when P_r spontaneously reverts back from refractory to active with rate $d2_{rf}$. P_a can switch to either P_u or P_r with rates K_{off} and K_{rf} , respectively:

$$\frac{dP_a}{dt} = K_{on} * \left(\frac{NTF^m}{kD_1^m + NTF^m} \right) * P_u + d2_{rf} * P_r - (K_{off} + K_{rf}) * P_a \quad [4]$$

Equation 5 describes the species P_r . Only species P_a can become P_r with rate K_{rf} , while P_r can revert back to either P_u or P_a with rates $d1_{rf}$ and $d2_{rf}$, respectively:

$$\frac{dP_r}{dt} = K_{rf} * P_a - (d1_{rf} + d2_{rf}) * P_r \quad [5]$$

The sum of P_u , P_a and P_r was modelled as a constant throughout the simulation. For a promoter with 4 REs, for example, the total was 4 multiplied by a factor 2, a scaling factor that was found to be needed to fit the data.

Equation 6 describes the assembly of the PIC. This occurs when the promoter is in the active state P_a . The rate of PIC assembly depends on NTF binding to one or more REs, as well as on the looping

efficiency (j_m^{-1}) of the DNA sequence between the REs and the TATA box. The PIC can additionally disassemble with rate d_{pic} :

$$\frac{dPIC}{dt} = \frac{K_{pic}}{j_m} * \left(\frac{NTF^m}{kD_1^m + NTF^m} \right) * P_a - d_{pic} * PIC \quad [6]$$

Equation 7 describes RNA transcription of the target gene, that is, formation of nascent RNA (nRNA). We model this process as a Hill function of the PIC concentration, where n is the Hill coefficient and kD_2 is the dissociation constant of the PIC components from the core promoter, multiplied by the rate constant K_{nrna} . We use a Hill function to model the cooperative binding of the general transcription factors that form the PIC. Additionally, the nRNA is released from the DNA template at rate d_{nRNA} :

$$\frac{dnRNA}{dt} = K_{nrna} * \left(\frac{[PIC]^n}{kD_2^n + [PIC]^n} \right) - d_{nRNA} * nRNA \quad [7]$$

Equation 8 describes the formation of mature RNA (mRNA). This is a function of the nascent RNA after it dissociates from the DNA template, and gets processed and translocated to the cytosol giving rise to the matured mRNA (mRNA) with rate $K_{prosRNA}$. To compensate for the fact that the nRNA visualization method we use gives only a rough estimate of the total transcribed RNA (that is, we can visualize only a focus when several nRNAs are present), we add a scaling factor f . We call the product of these two constants K_{mRNA} . We also assume that the mRNA gets degraded at a constant rate d_{mRNA} :

$$\frac{dmRNA}{dt} = K_{mRNA} * nRNA - d_{mRNA} * mRNA \quad [8]$$

Equation 9 describes ribosome loading on properly processed mRNA. This is modelled as a mass action function with rate K_{rbz} multiplied by the amount of translated mRNA. We assumed that not all mRNAs are translation-competent, hence a constant rt is subtracted from the mRNA amount. This term was deemed necessary because the model does not fit the 5'UTR constructs without it. mRNA-bound ribosomes can also dissociate at a fixed rate d_{rbz} :

$$\frac{drbz}{dt} = K_{rbz} * (mRNA - rt) - d_{rbz} * rbz \quad [9]$$

Equation 10 describes mRNA translation to an immature protein iP. We model this process as a function of the bound ribosomes multiplied by the constant K_{p1} . iP becomes mature protein mP at rate R_p and is degraded at rate d_p :

$$\frac{diP}{dt} = K_{p1} * rbz - (R_p + d_p) * iP \quad [10]$$

Finally, equation 11 describes the maturation of the fluorescent protein mP. mP gets degraded at rate d_{mp} :

$$\frac{dmP}{dt} = R_p * iP - d_{mp} * mP \quad [11]$$

The experimentally measured iRFP670 protein corresponds to the species mP.

Equation 12 describes how we calculate the factor j_m , and is based on previous work (2). L represents the distance between the TATA box and the last RE (that is, the RE closest to the TATA box) in bp, while P is the length of the DNA in nm. To calculate the length we use a previous estimate (2, 3):

$$j_m = \left(\frac{1.25e^5}{P^3} \right) * \left(\frac{4*P}{L*10^4} \right)^{\frac{3}{2}} * e^{-(510*P^2)/(6.25*L^2+50*P^2)} \quad [12]$$

The ODEs were written in python v3.8.3.final.0 using the Anaconda v2020.07 distribution. Numerical simulations were performed using the odeint function in SciPy v1.5.0 `scipy.integrate` module, which is used as a wrapper for the LSODA ordinary differential equation solver for stiff or non-stiff systems from the FORTRAN library `odepack`.

Initial conditions were set according to experimental observations or were fitted. Variables of interest were plotted using `matplotlib` plotting library.

Parameters

The model entails a total of 22 parameters if we consider the promoter-specific parameters. Except for kD_1 , kD_2 , d_{mRNA} and R_p , all parameters were first fitted together using experimental data obtained with promoter p2 under sustained dynamics, namely nascent RNA and reporter protein kinetics, as well as reporter protein expression at the end of the experiment under different NTF levels (Supplementary Figure S4). The parameter d_{mRNA} was experimentally calculated for different mRNAs (Supplementary Figure S5). Parameter fitting was done using both adaptive memory programming for global optimization (`ampgo`) and basin-hopping global optimization algorithms in the `lmfit.minimize` package in python. The parameter set that successfully predicted the nascent RNA and protein data for the remaining pulsatile dynamics (high- and low-frequency) was used for the other promoters. The values of m , K_{pic} , d_{pic} , K_{nrna} , d_{nrna} , d_{rbz} , K_{p1} , dp , and d_{mp} were fixed for all promoters. K_{mRNA} was, instead, fitted for all constructs (due to the fact that the scaling factor f might differ across constructs).

In the instances of modified 5' UTR, rt was re-estimated from experimental data, and K_{on} , K_{off} , K_{rf} , $d1_{rf}$, $d2_{rf}$, K_{mRNA} , and K_{rbz} were allowed to change, since we reasoned that changing 5' UTR affects the loading of ribosomes and the proportion of mRNA that is translated.

Parameter fitting

All parameter fittings were done with data from the sustained dynamics. Parameters were first fitted with the least square function (leastsq) from the lmfit.minimize python module. The resulting parameters were then used as the initial parameter guesses for global parameter fit using the adaptive memory programming for global optimization method (ampgo) or basinhopping algorithm implemented in lmfit.minimize python module. To improve on the global parameter values, the ampgo fitted output was used as initial guesses for another round of leastsq function fitting to find the local minima of the global parameters.

A promoter that responds more strongly to pulses than to sustained signal exists: theoretical analysis

From our data and previous studies (2, 4, 5), we can conclude that, whenever a promoter is activated by pulsatile dynamics, it is also activated by a sustained TF signal. In other words, from the building blocks that make a promoter (mostly the RE and the TATA box), it is not possible to obtain a variant that specifically filters sustained signals out, while responding to pulsatile ones. Wilson and colleagues showed, for the Ras/Erk pathway, that negative feedback can promote a band-pass filtering behaviour allowing target genes to be most efficiently activated by Erk pulses of specific frequencies (5). We asked ourselves if there could exist an alternative mechanism, involving no other molecule than the TF itself, which could allow a promoter to be better activated by pulsatile than sustained TF dynamics.

Recently, phase separation around genomic loci has been shown to play a regulatory role in gene expression (6–8). These studies relate condensate formation with enhanced activity of the transcriptional activators that localize in them. Theoretically, however, formation of condensates could have an inhibitory function as well: too high local TF concentrations could lead to a strong refractory response of the promoter, which could eventually enter into an inactive state. As a reminder, the refractory state is defined as the state of the promoter for which the PIC cannot be assembled despite the TF being bound at the RE(s), due to lack of GTFs locally available at the promoter to nucleate the PIC. Recent work by Chong and colleagues supports this notion (9). Here, the endogenous TF EWS::FLI1 is brought into condensates of different sizes by differentially overexpressing the EWS low complexity domain. Depending on the size of the condensates, the TF either activates or represses the reporter genes (9).

We sought to explore *in silico* whether this mechanism could make a promoter respond better to pulsatile than sustained TF dynamics. We modified the original mathematical model to include a fourth promoter state: inactive. We assume that the inactive state is reachable from the refractory state and that, from this inactive state, the promoter can go back to being in the unbound state (Supplementary Figure S9A). The rate at which the promoter switches from the inactive to the unbound state is a nonlinear inverse hill function of synTF concentration multiplied by the parameter D_{in} , which is a scaling factor that depends on how fast the TF dissociates from the promoter. With this modified model we scanned the values for D_{in} and the interval between pulses that would lead to higher reporter protein

levels at the end of the experiment (630 min) for pulses than sustained synTF signal (special case when the time between pulses = 0). We found several combinations of D_{in} and pulse frequencies that would lead to higher reporter protein levels in this case (Supplementary Figure S9B). We then took one such combination and simulated two dynamics for synTF: sustained and pulses of the selected frequency specified by the arrow in Figure 6B (55 min light activation followed by 25 min dark phase; $D_{in}= 0.0031$). Importantly, also in these simulations, we kept synTF cumulative levels constant, as done in the experiments. Therefore, the activation of synTF in the case of the pulsatile dynamics goes on for a longer time than for the sustained dynamics. We calculated the simulated mean nascent RNA levels over time for both dynamics. The model predicts that, while transcription rapidly decreases and eventually ceases for the sustained synTF signal, transcription goes on for the pulsatile synTF signal until there is no nuclear synTF (Supplementary Figure S9C). The predicted cumulative nascent RNA levels are, therefore, higher for the pulsatile than the sustained dynamics (Supplementary Figure S9D). The simulations show that a sustained synTF signal would lead to much lower reporter protein levels than the pulses (Supplementary Figure S9E). Taken together, the mathematical model indicates that it is possible for a promoter to be more efficiently activated by a pulsatile than a sustained TF signal, provided the TF inhibits PIC assembly when above a certain threshold.

Supplementary Table S1 Sequences and affinities of promoter elements used to design reporter constructs tested in this study

<i>Element</i>	<i>Sequence</i>	<i>Kd (nM)</i>
<i>strong RE</i>	CTGTATATAAAACCAGTGGTTATATGTACAGACTAGA	1.61
<i>weak RE</i>	CTGTAAAAAAAAAACAGTGGTTATATGTACAGACTAGA	5.64
<i>strong TATA</i>	AGACGCTATAAAAGGGATCC	2
<i>weak TATA</i>	AGAGGGTATATAATGGATCC	4
<i>seq1</i>	CTGTATATAAAACCAGTGGTTATATGTACAGACTAGACTCTG GACTCCTCCCCGGGTGTCGCTCCTTCATCTGACAATATGCA GCCGCTACCACCATCGATTAATAACAACGAACGGTGTATGTTG TCATAGATTCCGGCACATTTCCCTTGTAGGTGTGAAATCACTT AGCTTCGCGCCGAAGTCTTATGAGTCCGAGCGGAGACTCT AGAGGGTATATAAT	-
<i>seq2</i>	CTGTATATAAAACCAGTGGTTATATGTACAGACTAGACTCTG GAGAATCCCGGTCTGCAGGCCGCTCAATTGGTCGTAGACA GCTCTAGCACCGCTTAAACGCACGTACGCGCTGTCCCCCG CGTTTTAACCGCCAAGGGGATTACTCCCTAGTCTCCAGGCA CGTGTCAGATATATACATCCTGATGAGTCCGAGCGGAGACT CTAGAGGGTATATAA	-
<i>UTR1</i>	AGAGGGTATATAATCGGCTATGCACGAAGCAACTCTTGCCA CCATGGCGCGTAAGGT	-
<i>UTR2</i>	AGAGGGTATATAATCGGCTATGCACGAAGCAACTCTAACCA CCATGGCGCGTAAGGT	-
<i>UTR3</i>	AGAGGGTATATAATCGGCTATGCACGAAGCAACTCTTGAGT GTATGGCGCGTAAGGT	-
<i>UTR4</i>	AGAGGGTATATAATGGATCCCCGGGTACCGAGCTCGAATTC CAATGGCGC	-
<i>UTR5</i>	AGAGGGTATATAATCGGCTATGCACGAAGCAACTCTAACCA CCATGGCGC	-
<i>UTR6</i>	AGACGCTATAAAAGGGCGGTAAGTGGTAAATAGGCGCC ACCATGGCGC	-
<i>Stronger RE</i>	CTGTATATATATACAGTGGTTATATGTACAGACTAGA	0.8
<i>INR</i>	AGACTTTACATCTACTGTT	-

The red coloured nucleotides indicate the sequence of the elements.

Supplementary Table S2 Complete list of reporter constructs tested in this study

<i>Promoter</i>	<i>#RE</i>	<i>LexA affinity for RE (kD₁) (nM)</i>	<i>λ (bp)</i>	<i>TBP affinity for TATA box kD₂ (nM)</i>	<i>δ (bp)</i>	<i>REF</i>
<i>p1</i>	4	1.61	49	2 [*]	69	(10, 11)
<i>p2</i>	4	1.61	49	4 [*]	69	(10, 11)
<i>p3</i>	4	5.64	49	2	69	(11, 12)
<i>p4</i>	4	5.64	49	4	69	(11, 12)
<i>p5</i>	4	1.61	196 ^a	2	69	(10, 11)
<i>p6</i>	4	1.61	196 ^a	4	69	(10, 11)
<i>p7</i>	4	1.61	196 ^b	4	69	(10, 11)
<i>p8</i>	2	1.61	49	4	69	(10, 11)
<i>p9</i>	2	1.61	49	2	69	(10, 11)
<i>p10</i>	4	0.80	49 bp	2	69	(11, 12)
<i>p11</i>	4	0.80	49bp	4	69	(11, 12)
<i>p12</i>	2	0.80	49bp	4	69	(11, 12)
<i>p13</i>	4	1.61	343 ^c	4	69	(10, 11)
<i>p14</i>	4	1.61	343 ^c	2	69	(10, 11)
<i>p15</i>	4	0.80	343 ^c	2	31	(11, 12)
<i>p16</i>	8	1.61	343 ^c	4	69	(10, 11)
<i>p17</i>	4	1.61	343 ^d	4	69	(10, 11)
<i>p18</i>	2	1.61	196 ^a	4	69	(10, 11)
<i>p19^e</i>	4	1.61	49	N/A	69	(10, 11)
<i>p20^f</i>	4	1.61	49	N/A	31	(10, 11)
<i>p21^g</i>	4	1.61	49	N/A	69	(10, 11)
<i>5UTR1</i>	4	1.61	49	4	31 ^h	(10, 11)
<i>5UTR2</i>	4	1.61	49	4	31 ⁱ	(10, 11)
<i>5UTR3</i>	4	1.61	49	4	31 ^j	(10, 11)
<i>5UTR4</i>	4	1.61	49	4	31 ^k	(10, 11)
<i>5UTR5</i>	4	1.61	49	4	31 ^l	(10, 11)
<i>5UTR6</i>	4	1.61	49	2	31 ^m	(10, 11)
<i>5UTR7</i>	4	5.64	49	2	31 ⁿ	(11, 12)
<i>5UTR8</i>	4	1.61	49	N/A	31 ^o	(10, 11)

^{*} We have used values derived from experimental studies in yeast (11). Experimental data obtained using human TBP appear to lie in a similar range (13). ^a Insertion of seq1 between REs and TATA box.

^b Insertion of seq2 between REs and TATA box. ^c Insertion of 2x seq1 between REs and TATA box. ^d

Insertion of 2x seq1 flanked by the CTCF binding sequence on both 5' and 3' ends. ^e Promoter with

initiator sequence in place of TATA box combined by downstream promoter element. ^f Promoter with

2x initiator sequence (Inr) in place of the TATA box. ^g Promoter with 2x initiator sequence in place of the TATA-box. ^h Promoter p2 combined with optimal Kozak sequence. ⁱ Promoter p2 combined with suboptimal Kozak sequence. ^j Promoter p2 combined with a random sequence in place of the Kozak sequence. ^k Promoter p2 with 62% GC content between the TATA box and the start codon without Kozak sequence. ^l Promoter p2 with 55% GC content between the TATA box and the start codon combined with the suboptimal Kozak sequence. ^m Promoter p1 with 59% GC content between the TATA box and the start codon, and optimal Kozak sequence. ⁿ Promoter p4 with 59% GC content between the TATA box and the start codon, and optimal Kozak sequence. ^o Promoter p1 with the start codon, and optimal Kozak sequence without the TATA box.

Supplementary Table S3 List of plasmids used in this study

<i>Name</i>	<i>Backbone</i>	<i>Insert</i>	<i>Promoter</i>	<i>Source</i>
<i>pDN98</i>	pmCherry-N1	LexA DNA binding /VP48 /IkBa NES/mCherry/LINuS (biNLS10)	CMV	(14)
<i>pDN100</i>	pFR-Luc	Firefly luciferase	4x LexA operator based promoter	(14)
<i>pEA00</i>	pDN98	Full length LexA	CMV	This study
<i>pEAXX</i>	pDN100	iRFP670-CAAX	4x LexA operator based promoter	This study
<i>pEA01</i>	pEA00	4x-LexA0/iRFP670- CAAX/BGH terminator	p2	This study
<i>pEA02</i>	pEA00	Reversed 4x- LexA0/iRFP670- CAAX/BGH terminator	p2	This study
<i>pEA03</i>	pEA01	Reversed CMV-full length LexA /VP48 /IkBa NES/mCherry/LINuS (biNLS10)/ SV40 terminator	p2	This study
<i>pEA04</i>	pEA01	Promoter p1	-	This study
<i>pEA05</i>	pEA04	Promoter p3	-	This study
<i>pEA06</i>	pEA05	Promoter p4	-	This study
<i>pEA07</i>	pEA04	Promoter p5	-	This study
<i>pEA08</i>	pEA01	Promoter p6	-	This study
<i>pEA09</i>	pEA01	Promoter p7	-	This study
<i>pEA10</i>	pEA04	Promoter p8	-	This study
<i>pEA11</i>	pEA01	Promoter p9	-	This study
<i>pEA12</i>	pEA01	Promoter p10	-	This study
<i>pEA13</i>	pEA12	Promoter p11	-	This study
<i>pEA14</i>	pEA12	Promoter p12	-	This study
<i>pEA15</i>	pEA01	Promoter p13	-	This study
<i>pEA16</i>	pEA04	Promoter p14	-	This study
<i>pEA17</i>	pEA12	Promoter p15	-	This study
<i>pEA18</i>	pEA15	Promoter p16	-	This study

Supplementary Table S3 continued

<i>pEA19</i>	<i>pEA15</i>	<i>Promoter p17</i>	-	<i>This study</i>
<i>pEA20</i>	pEA08	Promoter p18	-	This study
<i>pEA21</i>	pEA01	Promoter p19	-	This study
<i>pEA22</i>	pEA01	Promoter p20	-	This study
<i>pEA23</i>	pEA04	Promoter p21	-	This study
<i>pEA24</i>	pEA01	Promoter p2 5UTR1	-	This study
<i>pEA25</i>	pEA01	Promoter p2 5UTR2	-	This study
<i>pEA26</i>	pEA01	Promoter p2 5UTR3	-	This study
<i>pEA27</i>	pEA01	Promoter p2 5UTR4	-	This study
<i>pEA28</i>	pEA01	Promoter p2 5UTR5	-	This study
<i>pEA29</i>	pEA04	Promoter p2 5UTR6	-	This study
<i>pEA30</i>	pEA06	Promoter p2 5UTR7	-	This study
<i>pEA31</i>	pEA01	Promoter p2 5UTR8	-	This study
<i>pEAm</i>	pEA01	IRES-SV40/NLS- MCP	-	This study
<i>pEAm00</i>	pEAm	12xMBS-PBS	-	This study
<i>pEAm01</i>	pEAm00	Minus BGH terminator	-	This study
<i>pEAm02</i>	pEAm01	Promoter p1	-	This study
<i>pEAm03</i>	pEAm01	Promoter p3	-	This study
<i>pEAm04</i>	pEAm01	Promoter p4	-	This study
<i>pEAm05</i>	pEAm01	Promoter p5	-	This study
<i>pEAm06</i>	pEAm01	Promoter p6	-	This study
<i>pEAm07</i>	pEAm01	Promoter p7	-	This study
<i>pEAm08</i>	pEAm01	Promoter p8	-	This study
<i>pEAm09</i>	pEAm01	Promoter p9	-	This study
<i>pEAm10</i>	pEAm01	Promoter p12	-	This study

Supplementary Table S4 List of primers

#	Primer sequence 5'-3'
1	tcgtgtggctgccggtgaaccacttctggcgcaacagcat
2	gtcggccggcccgcttctgtaattaagctggtccgctaccaccagccagtcgccgttgcg
3	gaaagcggcgggcccggcc
4	tggttcaccggcagccac
5	aaaagaagaaaaagaagtcaagacaaagtgtgaattatgtaggcggccgctcgagcatg
6	ggtggcgctattaccaac
7	gttgtaaataggcgccaccatggcgcgtaaggctgatc
8	ttgtctttgactctttttctctttttacccttatagcgttggtggggcggcgg
9	atagtaatcaattacggggtcattagttc
10	taataactaatgcatggcggaatac
11	ccgccatgcattagtattacagacggatcgggagatc
12	accccgttaattgattactatgctggcaagtgtagcggtc
13	atccccgggtaccgagctcgaattccagcttgca
14	gctcgttaccgggatcccttttatagcgtctagagtctccgctcggactcg
15	tgatcagacatgtatattggactgtaaaaaaaaacagtggttatatgtacagactagactgtaaaaaaaaacagt ggttatatgtacagactagactcgagtccgag
16	tccaatatacatgtctgatcactgttttttttacagtctagtctgtacatataaccactgttttttttacagtctagatgcgg ccgcgaa ttaatacaacgaacggtgatgtgtcatagattcggcacattccctgtaggtgtgaaatcacttagcttcgcgccg
17	aagtcttatgagtcggagcggagactc
18	tgacaacatcaccgttcgttattaatcgatggtgtagcggctgcatattgtcagatgaaggagcgacaccgg ggaggagtccagagtctagtctgtacata
19	cgtacgcgctgtcccccgcttttaaccgccaaggggattactccctagtctccaggcacgtgtcagatatatacat cctgatgagtcggagcggagactcta
20	cgcgggggacagcgcgtacgtgctttaaagcgggtgctagagctgtctacgaccaattgagcggcctgcagacc gggattctccagagtctagtctgtacatata
21	aattcgcggccgatctagactgtatataaaaccagtgatcagacatgtatattggactgtatataaaaccagtggt tatatgtacagactagactcgagtccgagcg
22	tctagatgcggccgcaattcgta
23	tatatacagtgatcagacatgtatattggactgtatatacagtggttatatgtacagactagactgtatataata cagtggttatatgtacagactagactcgagtccg
24	tccaatatacatgtctgatcactgtatatacagctagtctgtacatataaccactgtatatacagcttagat gcggccgcaattcgg
25	gcgtagctgcgcataagcaaatgacaattaaccactgtgtactcgttataacatctggcagttaaagtcgggaga ataggagccgagtcggagcggagactc
26	ttgcttatgcgagctacgccatcgcgaggccggtccggcgggcaagcatataaaagaagctcgtcacatcc acatagttgataagactcggcgcgaa

Supplementary Table S4 continued

27	<i>tgatcagacatgtatattggactgtatataaaaccagtggttatgtacagactagactgtatataaaacc agtgattcgcggccgcatctagactgt</i>
28	tccaatatacatgtctgatcactggtttatatacagctagctgtacatataaaccactggtttatatacagctcggtac ccggtcacagcttgtctg
29	gactcttactccctagcttggatccccgggtaccg
30	aagactagggagtaagagtctccgctcggactc
31	gactcttactccctagcttccggctactgttgtaaataagg
32	atggcgcgtaaggctgatctcacctcctcgatcgcgagccg
33	atcgacctacgcgccatggtggcaagagtgcctcgtgcatagccgattatataccctc
34	atcgacctacgcgccatggtggtagagtgcctcgtgcatagccgattatataccctc
35	atcgacctacgcgccatacactcaagagtgcctcgtgcatagccgattatataccctc
36	atggatccccgggtaccgagctcgaattccaatggcgcgtaaggctgatc
37	tggaattcgagctcggtagccggggatccattatataccctctagagtctccgctc
38	atcgacctacgcgccatggtggctcaggtgattcgtgcatagccgattatataccctctagagtctccgctcggac tcg
39	tggcgcctattaccaacagtaccgccctttatagcgtctagagtctccgctcggactc
40	ggtggcgcctattaccaacagtaccggaatcgcgccctctagagtctccgc
41	tcgctcgtccagattccagggttcatcagagcatgcatctagagggcc
42	tgctttctggcaataagtagcctagtagctacttccacctgaacctccctacataattacacactttgtctttg ac
43	acctaaatgctagagctcgtgatcagcctatagtaataattacggggtc
44	aggctgatcagcgagctc
45	agaagaaaaagctggactagatcgatggatccctcccccc
46	ccattttaacggctagcatgccaactttcttttcttttgggccatcctgcaggctg
47	atgctagccgttaaaatggcttctaac
48	atcccgtctagaatccgcgtag
49	ttctagacgggatccaccggtcgccaccatggtgagcaagggcgaggag
50	gattatgatctagagtgcggccgctcgagttactgtacagctcgtc

Supplementary Table S5 continued

<i>Parameter</i>	<i>p8</i>	<i>p9</i>	<i>5UTR1</i>	<i>5UTR2</i>	<i>5UTR3</i>
<i>iOn</i>	0.0514	0.0514	0.0514	0.0514	0.0514
<i>iOff</i>	0.0059	0.0059	0.0059	0.0059	0.0059
<i>rOn</i>	0.1948	0.1948	0.1948	0.1948	0.1948
<i>rOff</i>	0.0817	0.0817	0.0817	0.0817	0.0817
<i>KTF</i>	52.1835	52.1835	52.1835	52.1835	52.1835
<i>dTF</i>	0.0297	0.0297	0.0297	0.0297	0.0297
<i>dNTF</i>	0.0081	0.0081	0.0081	0.0081	0.0081
<i>m</i>	2.8445	2.8445	2.8445	2.8445	2.8445
<i>kD1</i>	161.18	161.18	161.18	161.18	161.18
<i>n</i>	2.33	1.60	1.71	1.71	1.71
<i>kD2</i>	400	200	400	400	400
<i>Kon</i>	0.0410	0.0484	0.0999	0.0999	0.0999
<i>Koff</i>	0.0300	0.0119	0.0941	0.0941	0.0941
<i>Krf</i>	0.0213	0.4924	0.1594	0.1594	0.1594
<i>d1rf</i>	3.11E-05	2.94E-02	1.41E-02	1.41E-02	1.41E-02
<i>d2rf</i>	0.0000	0.0037	0.0061	0.0061	0.0061
<i>Kpic</i>	8.48E-06	8.48E-06	8.48E-06	8.48E-06	8.48E-06
<i>dpic</i>	0.5560	0.5560	0.5560	0.5560	0.5560
<i>Knrna</i>	19.5869	19.5869	19.5869	19.5869	19.5869
<i>dnRNA</i>	0.0474	0.0474	0.0474	0.0474	0.0474
<i>KmRNA</i>	17.7182	19.3246	26.5994	26.5994	17.7182
<i>dmRNA</i>	0.2340	0.2340	0.2090	0.2090	0.2340
<i>rt</i>	0	0	170	165	415
<i>Krbz</i>	0.0057	0.0057	0.0166	0.0115	0.0100
<i>drbz</i>	0.3600	0.3600	0.3600	0.3600	0.3600
<i>Kp1</i>	2.5381	2.5381	2.5381	2.5381	2.5381
<i>dp</i>	1.87E-03	1.87E-03	1.87E-03	1.87E-03	1.87E-03
<i>dmp</i>	1.41E-04	1.41E-04	1.41E-04	1.41E-04	1.41E-04
<i>Rp</i>	2.31E-03	2.31E-03	2.31E-03	2.31E-03	2.31E-03

Supplementary Table S6 List of NF- κ B target genes and the corresponding binding sites in the promoter region.

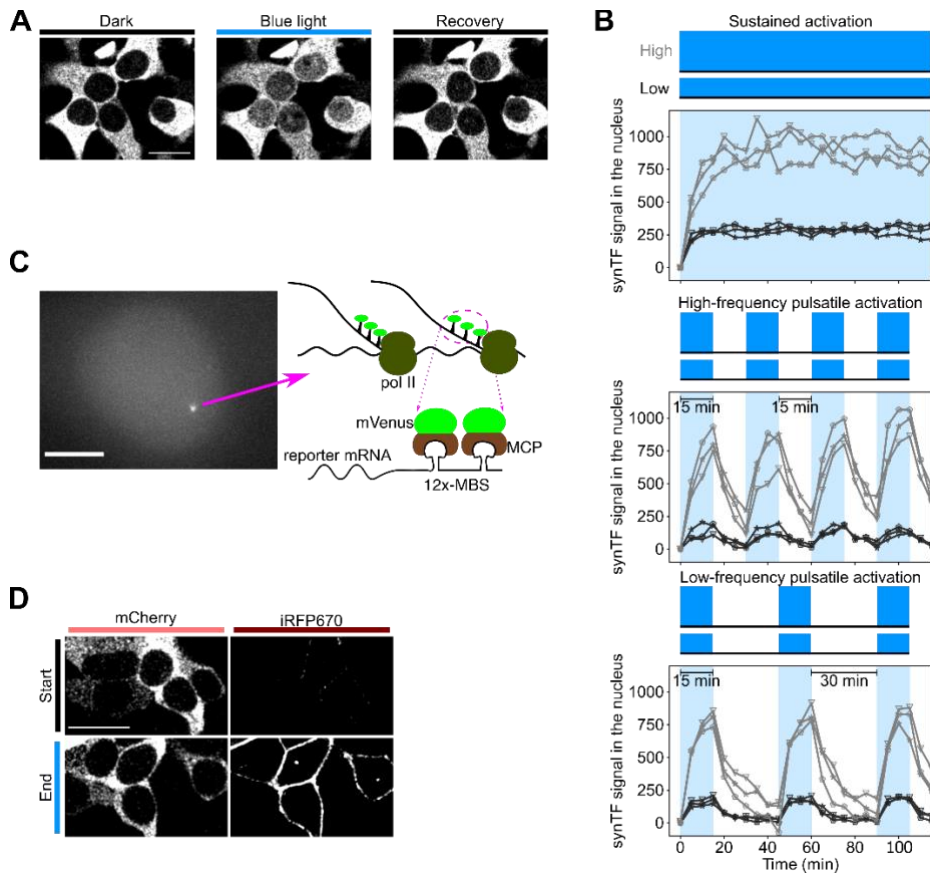
<i>Gene</i>	<i>NF-κB binding site</i>	<i>Reference</i>
<i>IL1A</i>	ctacaggggcatgccatcac gaggaggggctcccctcaca	(15)
<i>IL1B</i>	aacgtgggaaaatccagtat	(16)
<i>TNF</i>	ccccggggctgtcccaggct tgtgaggggatccttgatg ctcatgggttctccaccaa	(17–19)
<i>CXCL10</i>	gcagagggaaattccgtaac	(20)
<i>CXCL1</i>	actccgggaattccctggc	(21)
<i>CSF2</i>	gttcaggtagtccccgcc	(22)
<i>CXCL8</i>	tcgtggaattccttgaca	(23)
<i>IL6</i>	aatgtgggatttcccatga	(24, 25)
<i>NFKBIA</i>	tcggaaggacttccagcca ggcttgaaattccccgagc	(26)
<i>TRAF1</i>	accctgggattccaccag aaccaggggaactctactg acaaagggtaattcctgctc	(27)
<i>IFNG</i>	cgtctggaactccccctggg	(28)

Supplementary Table S7 List of p53 target genes and the corresponding binding sites in the promoter region.

<i>Genes</i>	<i>p53 responsive element</i>	<i>Reference</i>
<i>MDM2</i>	ggtaagtcagacacgttc agttaagtcctgactgtct	(29, 30)
<i>CDKN1A</i>	gaacatgtcccaacatgtg agactgggcatgtctggca	(31)
<i>BAX</i>	tcacaagttagagacaagcctgggcgtgggc	(32, 33)
<i>GADD45A</i>	gaacatgtctaagcatgctg	(34, 35)
<i>PML</i>	gcgctggcctggagccaggggcatgtcc	(36)
<i>YPEL3</i>	gggctcgggtgaaacaagtccaggcgctgcga	(37)
<i>APAF1</i>	agacatgtctggagaccctaggacgacaagccc aggcacgtccccagcgacagcaggctc	(38–40)
<i>BBC3</i>	ctgcaagtctgactgtcc	(34)
<i>XPC</i>	gaattgcccagacaagcaacatggct	(41)
<i>TP53AIP1</i>	tctctgcccgggctgtcg	(42)
<i>PPM1D</i>	ggcccagctctcgggacaagtcc	(43)

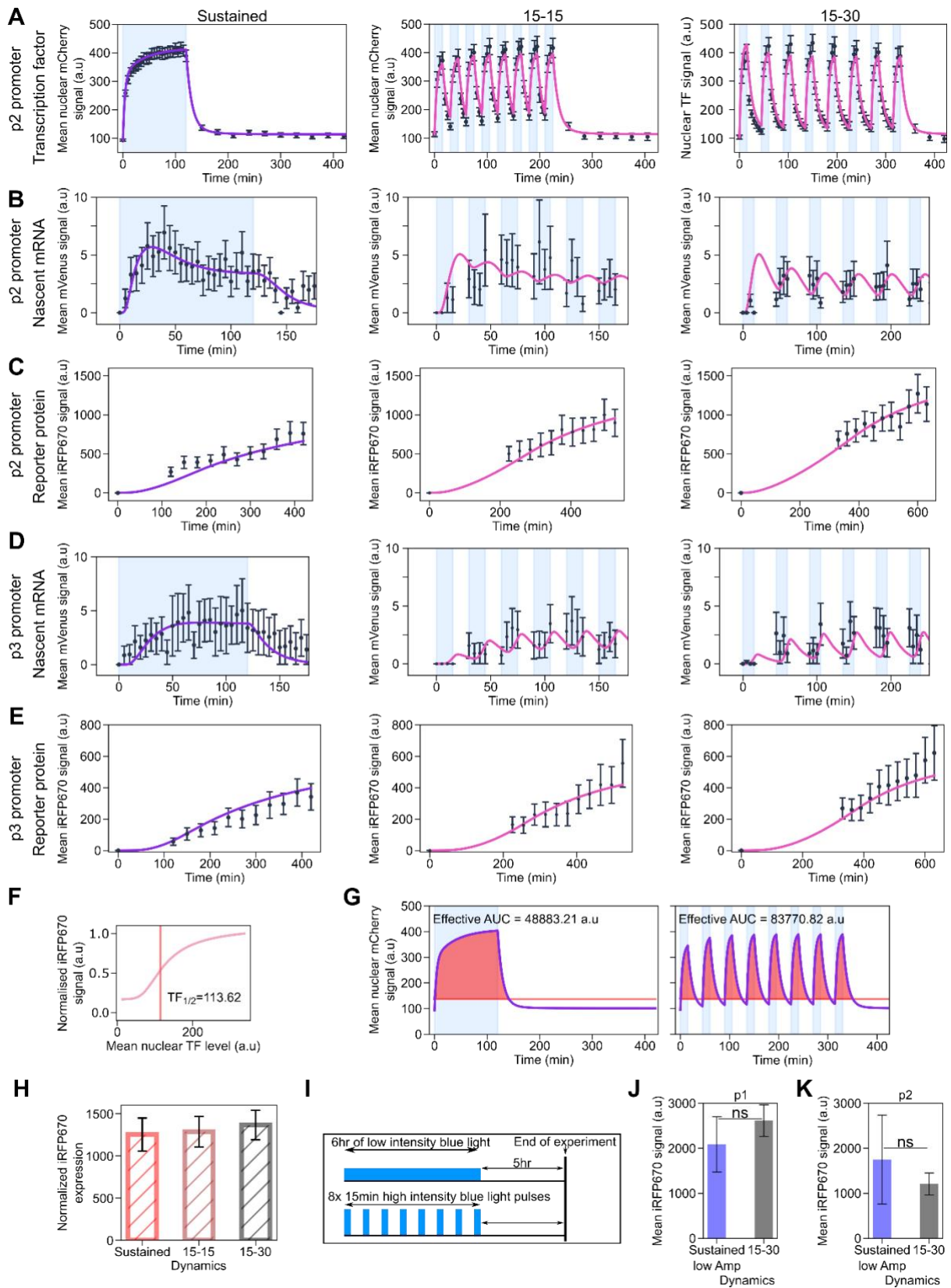
Supplementary Figures

Supplementary Figure S1



Experimental setup used in this study. **(A)** Representative fluorescence microscopy images showing accumulation of synTF in the nucleus of HEK293 cells upon blue light activation and recovery of cytoplasmic localization when the cells are kept in the dark. Illumination was performed shining 6.44 Wm^{-2} blue light for 125 msec every 45 sec for 15 min. Scale bar, 20 μm . **(B)** Generation of different TF dynamics with synTF. Graphs showing the nuclear TF signal over time in three distinct cells. Grey curves, high amplitude signal. Black curves, low amplitude signal. The low amplitude signal was achieved by illuminating the cells every 90 sec instead of every 45 sec. **(C)** Setup for live cell imaging of nascent RNA (nRNA). To monitor nRNAs in living cells, we deployed the MS2/MCP system (44, 45), comprising the bacteriophage MS2 capsid protein (MCP), fluorescently labeled by means of a genetic fusion to an FP (mVenus in our case), and multiple repeats of sequence-specific RNA stem loops (twelve in our case), which are integrated in the reporter transcript at the 5' or 3' UTR (3' UTR in our case). The stem loops are specifically bound by MCP, rendering the transcripts visible under the microscope at the site of transcription. Left, representative fluorescence microscopy image showing a fluorescent focus indicating the presence of several nRNAs. Scale bar, 5 μm . Right, schematic representation of the RNA visualization method used. MCP, MS2 coat protein. MBS, MCP binding site. MCP is expressed as a fusion to mVenus. **(D)** Representative fluorescence microscopy images of HEK293 cells showing synTF (mCherry) and reporter (iRFP670) levels before and after illumination with blue light. The reporter protein, iRFP670, is fused to the CAAX motif for plasma membrane localization. Scale bar, 20 μm .

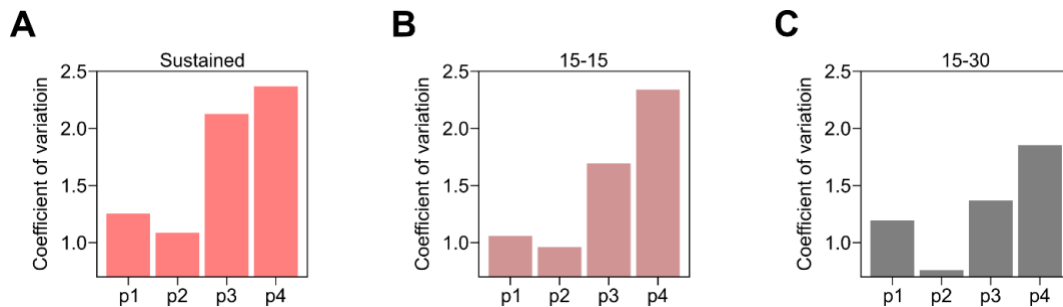
Supplementary Figure S2



Characterization of promoters p1, p2 and p3. **(A)** Quantification of synTF nuclear translocation over time for the indicated TF dynamics. **(B,D)** Quantification of mean reporter nascent RNA over time for the indicated TF dynamics. **(C,E)** Quantification of mean reporter protein levels over time for the indicated TF dynamics. (A-C) The promoter

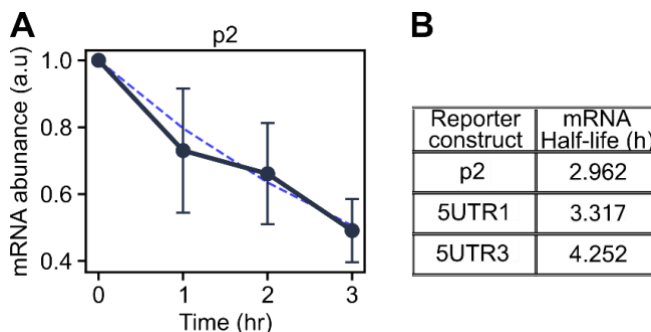
used in these experiment was p2. (D-E) The promoter used in these experiment was p3. (F) Prediction of synTF concentration above which the reporter protein is expressed above the half maximal value. (G) Calculation of the effective synTF cumulative levels using the threshold calculated in (F) for sustained (upper panel) and 15-30 pulsatile (lower panel) dynamics. (H) Quantification of mean reporter protein levels at the end of the experiment for the indicated synTF dynamics normalized using the effective cumulative synTF levels calculated in (G). (F-G) The promoter used was p1. (I) Schematic showing the experimental setup in which amplitude was varied to achieve similar cumulative synTF levels at fixed experimental time. (J,K) Quantification of mean reporter protein levels for the indicated TF dynamics for promoters p1 (J) and p2 (K). Light blue shadowing, blue light illumination phase. Together with the experimental data (black dots), fitted (violet line; for sustained dynamics) and simulated (pink line; for both pulsatile dynamics) values are shown. The mathematical model is shown in Figure 4 and the equations are described in the Supplementary Text. (A-E, H, J-K) Data represent mean \pm s.e.m. of at least n=20 individual cells, imaged on at least n=3 biologically independent experiments. P-values were calculated with the Welch's t-test. ns, non significant ($P > 0.05$).

Supplementary Figure S3



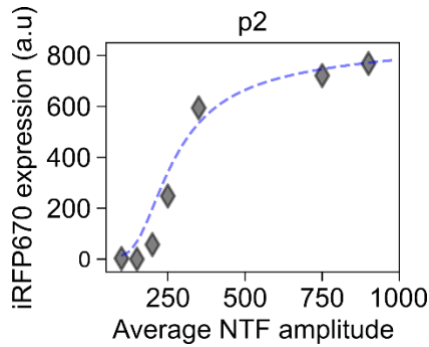
Promoters p3 and p4 are noisy. (A-C) Quantification of the coefficient of variation for the mean reporter protein levels at the end of the experiments for the indicated promoters under sustained (A), 15-15 (B) and 15-30 (C) pulsatile dynamics.

Supplementary Figure S4



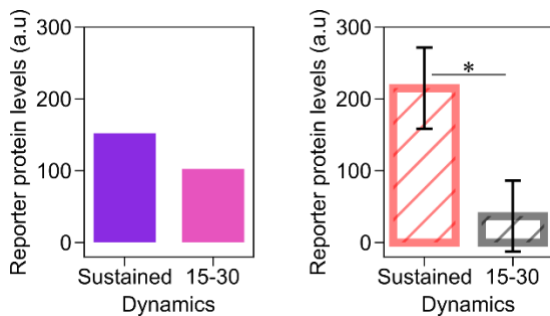
Experimental estimation of mRNA half-life. (A) Graph showing the mRNA levels measured via qPCR using the construct with the p2 promoter after addition of actinomycin D to the cells at time point t = 0. The experimental data are shown in black, the trend line in blue. Data represent the mean \pm s.d. of n=3 biologically independent experiments. (B) Estimated mRNA half-life for the three indicated reporter constructs.

Supplementary Figure S5



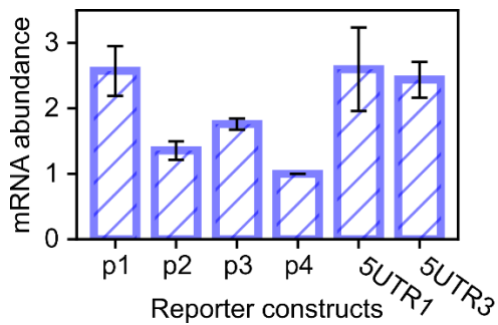
Reporter gene expression as a function of NTF concentration. Graph showing the amount of iRFP670 measured at the end of the experiment (5 h post sustained light activation, using promoter p2) in HEK293 cells expressing synTF in the nucleus at a certain concentration (indicated on the X-axis). Gray diamonds and blue dashed line represent experimental and fitted data, respectively. Data represent the mean of at least $n=20$ individual cells, imaged on at least $n=3$ biologically independent experiments.

Supplementary Figure S6



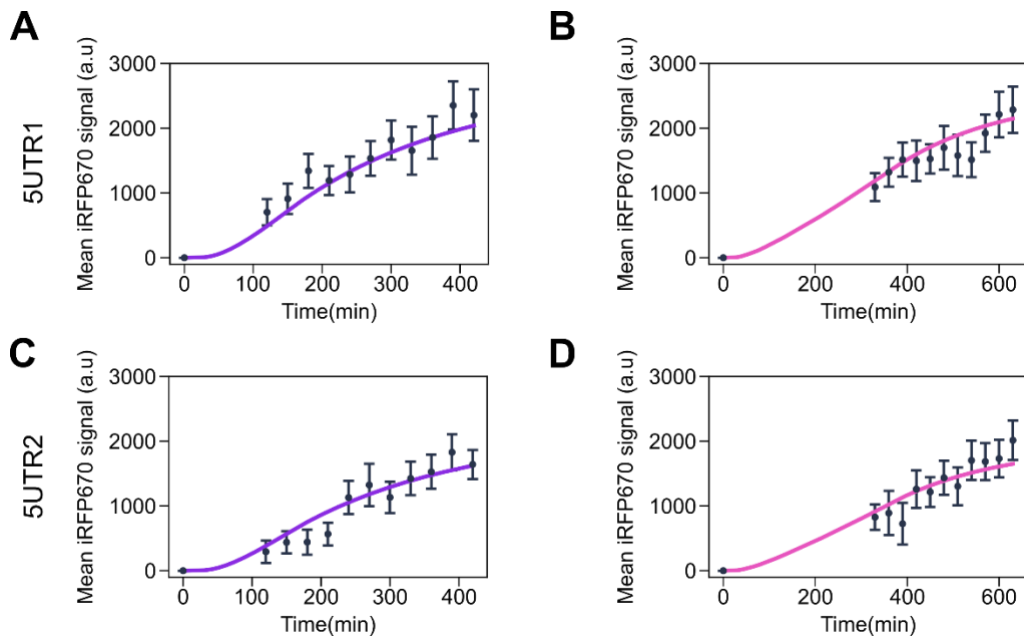
Promoter p2 with two instead of four REs senses dynamics also at the protein level. Model predictions (left panel; fitted (violet bar) and simulated (pink bar)), and experimental data (right panel) for the mean reporter protein levels at the end of the experiment for the indicated synTF dynamics in combination with promoter p9, which is a version of promoter p2 with two instead of four REs. Data represent mean \pm s.e.m. of at least $n=20$ individual cells, imaged on at least $n=3$ biologically independent experiments. P-values were calculated with the Welch's t-test. *, P-value = 0.01545.

Supplementary Figure S7



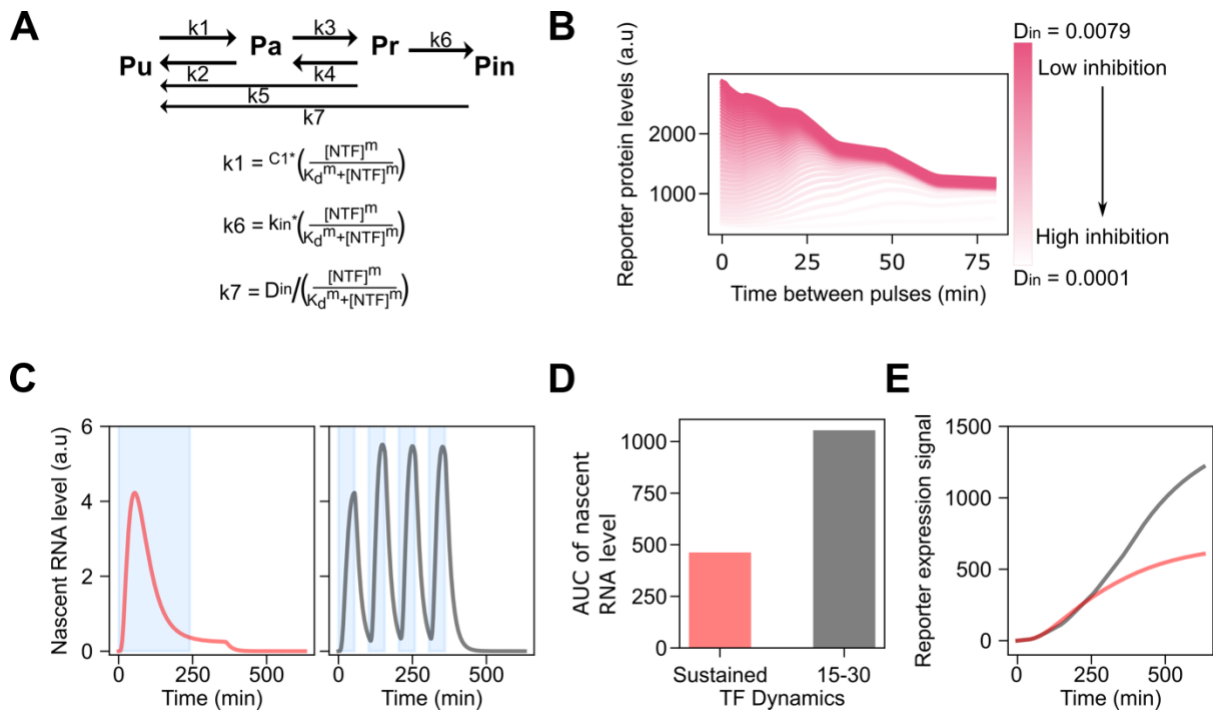
Relative mRNA abundance for different reporter constructs. Graph showing the mRNA levels measured by qPCR in HeLa cells transfected with the indicated constructs. Data represent mean \pm s.d. of $n=3$ biologically independent experiments.

Supplementary Figure S8



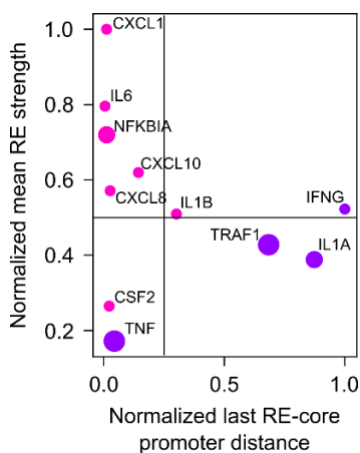
Measurements of mean reporter protein levels over time for constructs 5UTR1 and 5UTR2. (A-D) Quantification of mean reporter protein levels over time for sustained (A,C) and 15-30 pulsatile (B,D) dynamics for constructs 5UTR1 (A,B) and 5UTR2 (C,D). Data represent mean \pm s.e.m. of at least $n=20$ individual cells, imaged on at least $n=3$ biologically independent experiments. Lines represent simulations. Violet lines represent data fitting, while pink lines represent predictions.

Supplementary Figure S9



A promoter that filters out sustained signal, but is activated by pulses can theoretically exist. **(A)** Modified mathematical model that includes a fourth promoter state. Only the rates, which are different compared with the model without the fourth promoter state, are shown. **(B)** Simulated values of the reporter protein at the end of the experiment as a function of the interval between pulses for different values of the parameter D_{in} . When the time between pulses is zero the signal is sustained. Black arrow, selection of parameters used to simulate the system in (C-E). $D_{in} = 0.0007$. Time between pulses = 48 min. **(C)** Simulated nascent RNA levels for sustained (left panel) or pulsatile (right panel) dynamics using the model shown in (A) and the values for D_{in} and time between pulses selected in (B). Simulated area under the curve (AUC) for the nascent RNA for the indicated dynamics. **(E)** Simulated reporter protein levels over time for sustained (coral curve) or pulsatile (grey curve) TF dynamics.

Supplementary Figure S10



Promoter features allow the classification of NF- κ B-responsive promoters into sensitive and insensitive to dynamics. Plot showing NF- κ B-responsive promoters according to the distance between the last RE and the core promoter normalized to the longest distance (x-axis) and the mean RE strength normalized to the strongest RE (y-

axis). Each dot represents a promoter, color-coded to indicate activation by pulsatile (magenta) or sustained (violet) TF signal. The size of the dots increases with the number of REs.

Legend to Supplementary Video S1

Nascent RNA visualization for promoter p1 under sustained synTF dynamics. HEK293 cells expressing NLS-MCP-mVenus for the visualization of the target RNA were transiently transfected with the plasmid encoding synTF and the reporter gene iRFP670 under promoter p1. synTF was subjected to sustained dynamics. Nascent RNA was visualized every 5 min for two hours.

Supplementary References

1. Yao,X., Rosen,M.K. and Gardner,K.H. (2008) Estimation of the available free energy in a LOV2-Ja photoswitch. *Nat. Chem. Biol.*, **4**, 491–497.
2. Li,C., Cesbron,F., Oehler,M., Brunner,M. and Höfer,T. (2018) Frequency Modulation of Transcriptional Bursting Enables Sensitive and Rapid Gene Regulation. *Cell Syst.*, **6**, 409-423.e11.
3. Ringrose,L., Chabanis,S., Angrand,P.O., Woodroffe,C. and Stewart,A.F. (1999) Quantitative comparison of DNA looping in vitro and in vivo: Chromatin increases effective DNA flexibility at short distances. *EMBO J.*, **18**, 6630–6641.
4. Hansen,A.S. and O'Shea,E.K. (2013) Promoter decoding of transcription factor dynamics involves a trade-off between noise and control of gene expression. *Mol. Syst. Biol.*, **9**, 704.
5. Wilson,M.Z., Ravindran,P.T., Lim,W.A. and Toettcher,J.E. (2017) Tracing Information Flow from Erk to Target Gene Induction Reveals Mechanisms of Dynamic and Combinatorial Control. *Mol Cell*, **67**, 757-769 e5.
6. Sen,S., Cheng,Z., Sheu,K.M., Chen,Y.H. and Hoffmann,A. (2020) Gene Regulatory Strategies that Decode the Duration of NFkappaB Dynamics Contribute to LPS- versus TNF-Specific Gene Expression. *Cell Syst*, **10**, 169-182 e5.
7. Shrinivas,K., Sabari,B.R., Coffey,E.L., Klein,I.A., Boija,A., Zamudio,A. V, Schuijers,J., Hannett,N.M., Sharp,P.A., Young,R.A., *et al.* (2019) Enhancer Features that Drive Formation of Transcriptional Condensates. *Mol Cell*, **75**, 549-561 e7.
8. Cai,D., Feliciano,D., Dong,P., Flores,E., Gruebele,M., Porat-Shliom,N., Sukenik,S., Liu,Z. and Lippincott-Schwartz,J. (2019) Phase separation of YAP reorganizes genome topology for long-term YAP target gene expression. *Nat Cell Biol*, **21**, 1578–1589.
9. Chong,S., Graham,T.G.W., Dugast-Darzacq,C., Dailey,G.M., Darzacq,X. and Tjian,R. (2022) Tuning levels of low-complexity domain interactions to modulate endogenous oncogenic transcription. *Mol. Cell*, 10.1016/J.MOLCEL.2022.04.007.
10. Lewis,L.K., Harlow,G.R., Gregg-Jolly,L.A. and Mount,D.W. (1994) Identification of high affinity binding sites for LexA which define new DNA damage-inducible genes in Escherichia coli. *J. Mol. Biol.*, **241**, 507–523.
11. Hahn,S., Buratowski,S., Sharp,P.A. and Guarente,L. (1989) Yeast TATA-binding protein TFIID binds to TATA elements with both consensus and nonconsensus DNA sequences. *Proc. Natl. Acad. Sci.*, **86**, 5718–5722.
12. Zhang,A.P.P., Pigli,Y.Z. and Rice,P.A. (2010) Structure of the LexA–DNA complex and implications for SOS box measurement. *Nature*, **466**, 883–886.
13. Ponomarenko,P.M., Savinkova,L.K., Drachkova,I.A., Lysova,M. V., Arshinova,T. V.,

- Ponomarenko,M.P. and Kolchanov,N.A. (2008) A step-by-step model of TBP/TATA box binding allows predicting human hereditary diseases by single nucleotide polymorphism. *Dokl. Biochem. Biophys.*, **419**, 88–92.
14. Niopek,D., Benzinger,D., Roensch,J., Draebing,T., Wehler,P., Eils,R. and Di Ventura,B. (2014) Engineering light-inducible nuclear localization signals for precise spatiotemporal control of protein dynamics in living cells. *Nat. Commun.*, **5**, 4404.
 15. Mori,N. and Prager,D. (1996) Transactivation of the Interleukin-1 α Promoter by Human T-Cell Leukemia Virus Type I and Type II Tax Proteins. *Blood*, **87**, 3410–3417.
 16. Hiscott,J., Marois,J., Garoufalidis,J., Roulston,A., Kwan,I., Pepin,N., Lacoste,J., Nguyen,H., Bensi,G. and Fenton,Mati. (1993) Characterization of a functional NF-kappa B site in the human interleukin 1 beta promoter: evidence for a positive autoregulatory loop. *Mol. Cell. Biol.*, **13**, 6231.
 17. Shakhov,A.N., Collart,M.A., Vassalli,P., Nedospasov,S.A. and Jongeneel,C. V. (1990) Kappa B-type enhancers are involved in lipopolysaccharide-mediated transcriptional activation of the tumor necrosis factor alpha gene in primary macrophages. *J. Exp. Med.*, **171**, 35–47.
 18. Collart,M.A., Baeuerle,P. and Vassalli',P. (1990) Regulation of tumor necrosis factor alpha transcription in macrophages: involvement of four kappa B-like motifs and of constitutive and inducible forms of NF-kappa B. *Mol. Cell. Biol.*, **10**, 1498–1506.
 19. Yao,J., Mackman,N., Edgington,T.S. and Fan,S.T. (1997) Lipopolysaccharide Induction of the Tumor Necrosis Factor- α Promoter in Human Monocytic Cells: REGULATION BY Egr-1, c-Jun, AND NF- κ B TRANSCRIPTION FACTORS. *J. Biol. Chem.*, **272**, 17795–17801.
 20. Harris,D.P., Bandyopadhyay,S., Maxwell,T.J., Willard,B. and DiCorleto,P.E. (2014) Tumor necrosis factor (TNF)- α induction of CXCL10 in endothelial cells requires protein arginine methyltransferase 5 (PRMT5)-mediated nuclear factor (NF)- κ B p65 methylation. *J. Biol. Chem.*, **289**, 15328–15339.
 21. Anisowicz,A., Messineo,M., Lee,S.W., Sager',R. and Sager,R. (1991) An NF-kappa B-like transcription factor mediates IL-1/TNF-alpha induction of gro in human fibroblasts. *J. Immunol.*, **147**, 520–527.
 22. Schreck,R. and Baeuerle,P.A. (1990) NF-kappa B as inducible transcriptional activator of the granulocyte-macrophage colony-stimulating factor gene. *Mol. Cell. Biol.*, **10**, 1281–1286.
 23. Mukaida,N., Mahe,Y. and Matsushima,K. (1990) Cooperative interaction of nuclear factor-kappa B- and cis-regulatory enhancer binding protein-like factor binding elements in activating the interleukin-8 gene by pro-inflammatory cytokines. *J. Biol. Chem.*, **265**, 21128–21133.
 24. Matsusaka,T., Fujikawa,K., Nishio,Y., Mukaida,N., Matsushima,K., Kishimoto,T. and Akira,S. (1993) Transcription factors NF-IL6 and NF-kappa B synergistically activate transcription of the inflammatory cytokines, interleukin 6 and interleukin 8. *Proc. Natl. Acad. Sci. U. S. A.*, **90**, 10193–10197.

25. Libermann,T.A. and Baltimore,D. (1990) Activation of interleukin-6 gene expression through the NF-kappa B transcription factor. *Mol. Cell. Biol.*, **10**, 2327.
26. De Martin,R., Vanhove,B., Cheng,Q., Hofer,E., Csizmadia,V., Winkler,H. and Bach,F.H. (1993) Cytokine-inducible expression in endothelial cells of an I kappa B alpha-like gene is regulated by NF kappa B. *EMBO J.*, **12**, 2773–2779.
27. Schwenzler,R., Siemienski,K., Liptay,S., Schubert,G., Peters,N., Scheurich,P., Schmid,R.M. and Wajant,H. (1999) The human tumor necrosis factor (TNF) receptor-associated factor 1 gene (TRAF1) is up-regulated by cytokines of the TNF ligand family and modulates TNF-induced activation of NF-kappaB and c-Jun N-terminal kinase. *J. Biol. Chem.*, **274**, 19368–19374.
28. Sica,A., Dorman,L., Viggiano,V., Cippitelli,M., Ghosh,P., Rice,N. and Young,H.A. (1997) Interaction of NF-κB and NFAT with the interferon-γ promoter. *J. Biol. Chem.*, **272**, 30412–30420.
29. Zauberman,A., Flusberg,D., Haupt,Y., Barak,Y. and Oren,M. (1995) A functional p53-responsive intronic promoter is contained within the human mdm2 gene. *Nucleic Acids Res.*, **23**, 2584–2592.
30. Riley,T., Sontag,E., Chen,P. and Levine,A. (2008) Transcriptional control of human p53-regulated genes. *Nat. Rev. Mol. Cell Biol.*, **9**, 402–412.
31. Resnick-Silverman,L., St. Clair,S., Maurer,M., Zhao,K. and Manfredi,J.J. (1998) Identification of a novel class of genomic DNA-binding sites suggests a mechanism for selectivity in target gene activation by the tumor suppressor protein p53. *Genes Dev.*, **12**, 2102.
32. Thornborrow,E.C., Patel,S., Mastropietro,A.E., Schwartzfarb,E.M. and Manfredi,J.J. (2002) A conserved intronic response element mediates direct p53-dependent transcriptional activation of both the human and murine bax genes. *Oncogene*, **21**, 990–999.
33. Chen,Y., Zhang,X., Dantas Machado,A.C., Ding,Y., Chen,Z., Qin,P.Z., Rohs,R. and Chen,L. (2013) Structure of p53 binding to the BAX response element reveals DNA unwinding and compression to accommodate base-pair insertion. *Nucleic Acids Res.*, **41**, 8368.
34. Pan,Y. and Nussinov,R. (2010) Lysine120 interactions with p53 response elements can allosterically direct p53 organization. *PLoS Comput. Biol.*, **6**.
35. Harris,C.R., Dewan,A., Zupnick,A., Normart,R., Gabriel,A., Prives,C., Levine,A.J. and Hoh,J. (2009) p53 responsive elements in human retrotransposons. *Oncogene 2009 2844*, **28**, 3857–3865.
36. De Stanchina,E., Querido,E., Narita,M., Davuluri,R. V., Pandolfi,P.P., Ferbeyre,G. and Lowe,S.W. (2004) PML Is a Direct p53 Target that Modulates p53 Effector Functions. *Mol. Cell*, **13**, 523–535.
37. Kelley,K.D., Miller,K.R., Todd,A., Kelley,A.R., Tuttle,R. and Berberich,S.J. (2010) YPEL3, a p53-regulated gene that induces cellular senescence. *Cancer Res.*, **70**, 3566.
38. Robles,A.I., Bemmels,N.A., Foraker,A.B. and Harris,C.C. (2001) APAF-1 Is a Transcriptional Target of p53 in DNA Damage-induced Apoptosis. *CANCER Res.*, **61**, 6660–6664.

39. Koh,D.I., An,H., Kim,M.Y., Jeon,B.N., Choi,S.H., Hur,S.S. and Hur,M.W. (2015) Transcriptional activation of APAF1 by KAISO (ZBTB33) and p53 is attenuated by RelA/p65. *Biochim. Biophys. Acta - Gene Regul. Mech.*, **1849**, 1170–1178.
40. Fortin,A., Cregan,S.P., MacLaurin,J.G., Kushwaha,N., Hickman,E.S., Thompson,C.S., Hakim,A., Albert,P.R., Cecconi,F., Helin,K., *et al.* (2001) APAF1 is a key transcriptional target for p53 in the regulation of neuronal cell death. *J. Cell Biol.*, **155**, 207.
41. Hastak,K., Adimoolam,S., Trinklein,N.D., Myers,R.M. and Ford,J.M. (2012) Identification of a Functional In Vivo p53 Response Element in the Coding Sequence of the Xeroderma Pigmentosum Group C Gene. *Genes Cancer*, **3**, 131–140.
42. Ma,B., Pan,Y., Zheng,J., Levine,A.J. and Nussinov,R. (2007) Sequence analysis of p53 response-elements suggests multiple binding modes of the p53 tetramer to DNA targets. *Nucleic Acids Res.*, **35**, 2986.
43. Rossi,M., Demidov,O.N., Anderson,C.W., Appella,E. and Mazur,S.J. (2008) Induction of PPM1D following DNA-damaging treatments through a conserved p53 response element coincides with a shift in the use of transcription initiation sites. *Nucleic Acids Res.*, **36**, 7168–7180.
44. Garcia,H.G., Tikhonov,M., Lin,A. and Gregor,T. (2013) Quantitative Imaging of Transcription in Living *Drosophila* Embryos Links Polymerase Activity to Patterning. *Curr. Biol.*, **23**, 2140–2145.
45. Larson,D.R., Zenklusen,D., Wu,B., Chao,J.A. and Singer,R.H. (2011) Real-time observation of transcription initiation and elongation on an endogenous yeast gene. *Science (80-.)*, **332**, 475–478.